Jaeheung Park
Oussama Khatib

Artificial Intelligence Laboratory
Stanford University
Stanford, CA 94305, USA
{park73,ok}@robotics.stanford.edu

A Haptic Teleoperation Approach Based on Contact Force Control

Abstract

This paper presents a new teleoperation approach using a virtual spring, and local contact force control on the slave robot. The operational space framework provides the control structure needed to achieve decoupled task dynamics. A virtual spring connects the master and slave systems and a closed-loop force controller compensates for the dynamics of the slave system, rendering transparent the effector of the slave robotic system. The active force control approach allows the desired motion and contact forces to be combined in a single force command. The required performance and robustness of force control are achieved by a full state reconstruction using a modified Kalman estimator, which addresses disturbances and modeling uncertainties. The performance of both telepresence and force control are further improved by on-line stiffness estimation of the object in contact with the effector. The redundancy of the mobile manipulation system is addressed through a decoupled decomposition of task and posture dynamics.

KEY WORDS—teleoperation, mobile manipulation, haptics, force control

1. Introduction

Haptic teleoperation provides telepresence by allowing a user to remotely control a slave robot through a master device while feeling the remote environment. These systems offer great potential, but connecting master/slave stations in a coherent way is a challenging task. While the master station is controlled by the human operator, the slave station often interacts with an unknown and dynamic environment. The nature of this interaction greatly influences overall system performance.

Many teleoperation schemes have been developed to improve telepresence and stability when position and force measurements are available on both the master and slave (Kim, Hannaford, and Bejczy 1992; Lawrence 1993; Zhu and Salcudean 2000). Telepresence is achieved when transparency

of the teleoperation system is realized, i.e., position tracking in free space operation, and force or impedance matching in contact (Lawrence 1993; Yokokohji and Yoshikawa 1994; Hashtrudi-Zaad and Salcudean 2002). A common control architecture is to use PD type position feedback control with direct feedforward force control to track the position and contact force of the counterpart system. This approach would provide perfect telepresence and stability in the ideal situation where the measurement of acceleration is available and the feedforward contact force is perfectly applied (Lawrence 1993; Yokokohji and Yoshikawa 1994). However, in practice, these conditions are not easily met. Specifically, the feedforward contact force command may not be realized due to many uncertainties such as friction characteristics and modeling errors. To address this difficulty, local force control is proposed in (Anderson and Spong 1989; Hannaford 1989; Kim, Hannaford, and Bejczy 1992; Yokokohji and Yoshikawa 1994; Hashtrudi-Zaad and Salcudean 2002) . One of the main challenges in this approach is to design a local force controller that works for an environment that is not known a priori (Hannaford 1989). Also, the overall stability is degraded when the measured contact force of one system is used as the desired contact force of its counterpart. This problem is exacerbated if the mass properties of the master and slave differ significantly (Daniel and McAree 1998). Another inherent characteristic of teleoperation systems is time delay in the communication link. Enhanced robustness to time delays using local force control is presented in Hashtrudi-Zaad and Salcudean (2002). To guarantee the stability of the overall system, passivity-based approaches have been extensively studied (Anderson and Spong 1989; Niemeyer and Slotine 1991, 2004; Ryu, Kwon, and Hannaford 2004); however, loss of performance is inevitable in this approach.

A new teleoperation approach is realized by integrating three components: a virtual spring to connect the master and slave systems, the operational space framework to provide the decoupled dynamic controller, and a local contact force controller to realize tracking of the contact force. This approach is illustrated in Figure 1 and the block diagram is in Figure 2. In the proposed teleoperation approach, a *virtual spring*
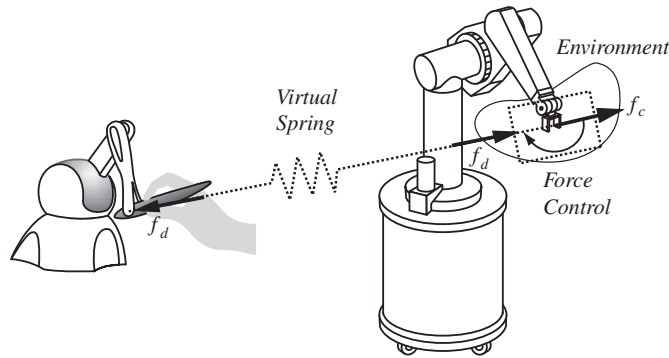
Fig. 1. Teleoperation approach with a virtual spring and force control. The desired force, f_d, is produced by the virtual spring based upon the position difference between the master and slave robot end-effectors. The force controller on the slave robot enforces the contact force, f_c, to track this desired force while the desired force is fed-back to the user at the master device.
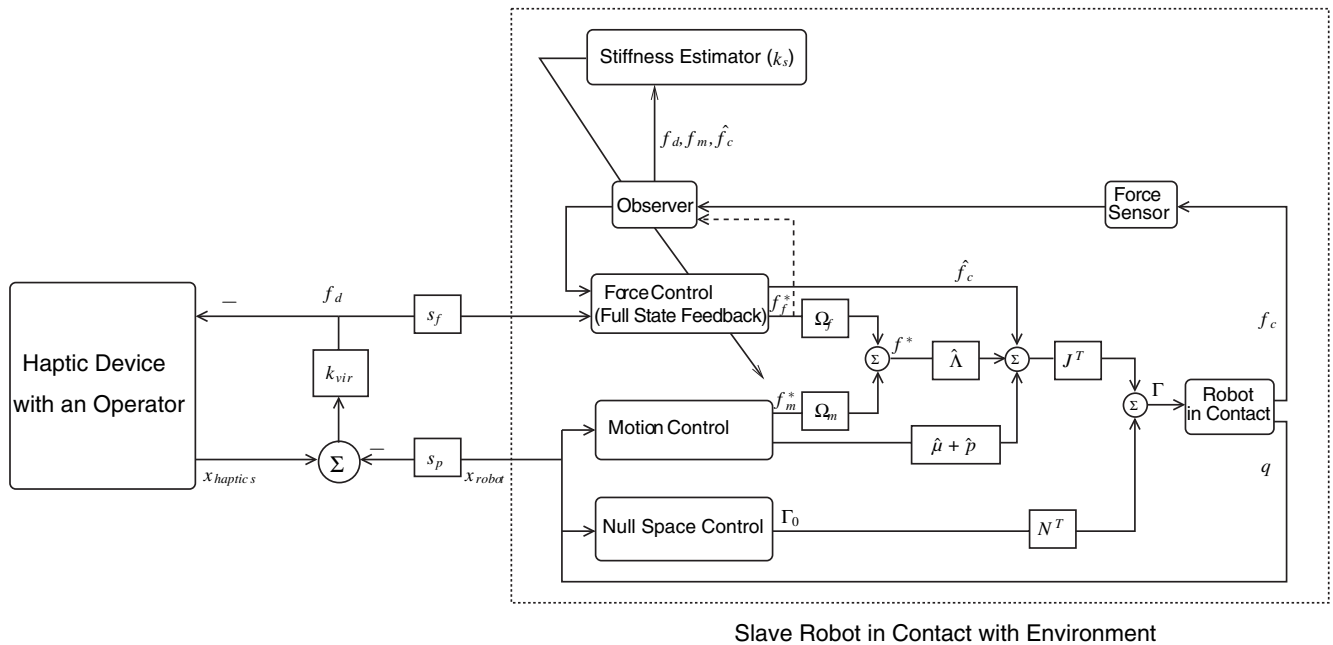

Fig. 2. A block diagram for the proposed teleoperation approach. The master and slave system are connected by a virtual spring with a spring constant, k_{vir}. The terms, s_p and s_f, are the scale factors for position and force, which are used to adjust different workspaces and force magnitudes for the two systems. The block diagram in the dotted block on the right side shows the motion/force control structure for redundant robots. This is described in Section 2.

connects the master and slave systems. When the positions of the master and slave system do not match, the virtual spring produces a force proportional to the difference in positions. This force acts as a desired contact force which will be tracked by local force control on each side. Therefore, this approach provides the human operator with contact forces within the bandwidth of the force controller. The robot control on each system is simply contact force control. Even in the free space operation of the slave system, the controller assumes that the robot is in contact with a very compliant environment.

The position tracking in free space is implicitly accomplished by the force control and the virtual spring. When the slave robot is in free space, the force control at the slave robot commands the robot to move toward the master's position until the difference in positions is zero since the virtual spring produces the desired contact force in that direction. This approach greatly simplifies the overall teleoperation architecture by connecting a virtual spring between the master and slave and incorporating local force control on each system. Furthermore, the stability characteristics with respect to time delays and the difference between the inertial properties of the master and slave system are improved since the measured contact force is not used as the desired contact force at the counterpart system. Moreover, no switching is required in the robot control structure since the robot is considered to be always in contact with the environment, even in free space.

Local force control is the most important part of the proposed approach since telepresence depends on how much bandwidth the force controller has. Also, implementation on a complex mobile manipulation system is not trivial. The operational space formulation (Khatib 1987) decouples the dynamics of the mobile manipulator into end-effector task dynamics and posture dynamics. Furthermore, each end-effector DOF can be independently controlled. The control of the base can be separately synthesized since its dynamics are decoupled from that of the end-effector. Based on this formulation, a local force control and teleoperation approach is applied for each end-effector DOF.

To deal with uncertainties and time-varying parameters (e.g. dynamic environments), the force control on the slave robot uses Active Observers (AOBs; Cortesão 2002) that modify the Kalman estimation structure to achieve model-reference adaptive control. The AOB is designed to cover a medium range of stiffness values. For large variations, on-line stiffness estimation is necessary (Cortesão, Park, and Khatib 2003). This on-line stiffness estimation is important in order to produce a desired bandwidth of the force controller over different environments, such that the teleoperation system can provide the user with a contact force. In addition, the virtual spring stiffness is modified with the change in the estimated environmental stiffness for better telepresence.

This architecture is especially suited for systems where force sensing is limited to the slave robot and when the master device is relatively light and frictionless. Specifically,

our setup, which uses a Phantom device and a PUMA robot mounted on a mobile base, meets this criteria. While it is imperative to use local force control on the slave mobile manipulation system, the light-weight frictionless haptic device generates relatively accurate commanded forces. Time delay associated with the wireless LAN network is also analyzed for our system.

Section 2 describes the overall control structure of a mobile manipulation system. Section 3 provides the force controller that is essential in the proposed teleoperation approach. The teleoperation approach is then given in Section 4. The experimental setup is described in Section 5 and the results are shown in Section 6. This paper is concluded in Section 7.

2. Control for a Mobile Manipulator

The dynamic equation of a mobile manipulator is described by

$$A(q)\ddot{q} + b(q, \dot{q}) + g(q) + J(q)^T f_c = \Gamma, \qquad (1)$$

where $q, A(q), b(q, \dot{q})$, and $g(q)$ are the vector of joint angles, the mass/inertia matrix, the Coriolis/centrifugal torque, and the gravity torque in joint space, respectively. The term, J, denotes the Jacobian for the contact point, which is the control point for the operational space coordinate. The term, f_c, is the vector of contact forces at the contact point. The term, Γ, is the vector of joint torques. The equations of motion for the end-effector of a robotic manipulator can be described using the operational space formulation (Khatib 1987). This yields

$$\Lambda(q)\dot{\vartheta} + \mu(q, \dot{q}) + p(q) + f_c = F \qquad (2)$$

where $\Lambda(q)$, $\mu(q, \dot{q})$, and $p(q)$ are the inertia matrix, the vector of Coriolis/centrifugal forces, and the vector of gravity forces in operational space, respectively. The term, ϑ, denotes the instantaneous linear and angular velocity in operational space coordinates. The term, F, is the control force at the operational point that is generated by the commanded torque, Γ. The control torque is selected as,

$$\begin{aligned} \Gamma &= J^T F + N^T \Gamma_0 & (3) \\ F &= \hat{\Lambda}(q) f^* + \hat{\mu}(q, \dot{q}) + \hat{p}(q) + \hat{f}_c & (4) \end{aligned}$$

where N^T is the dynamically consistent null space projection matrix (Khatib 1987) and f^* is the command to the unit mass system. The $\hat{}$ indicates an estimate of a particular quantity. The following decoupled equations of motion for the end-effector are obtained when the estimates are perfect.

$$\dot{\vartheta} = f^* \qquad (5)$$

The command f^* is composed of force and motion control components that are projected by the selection matrices, Ω_f and Ω_m, respectively.

$$f^* = \Omega_f f_f^* + \Omega_m f_m^* \qquad (6)$$

The subscripts f and m correspond to the force and motion control, respectively.

In the experimental setup, force control is used to control only the translational directions of the end-effector since the master device does not provide force feedback on the orientation. Therefore, the orientation of the end-effector is controlled by motion controller. When ϑ are composed of the translational and rotational velocities, the selection matrices are

$$\Omega_f = \begin{bmatrix} I_3 & 0_3 \\ 0_3 & 0_3 \end{bmatrix}, \qquad \Omega_m = \begin{bmatrix} 0_3 & 0_3 \\ 0_3 & I_3 \end{bmatrix} \qquad (7)$$

where I_3 is the 3×3 identity matrix and 0_3 is the 3×3 zero matrix. Motion control on f_m^* is implemented by PD control and force control on f_f^* will be described in Section 3.

The control of the mobile base is applied to Γ_0 in eq. (3). The dynamically consistent null space projection matrix N^T prevents control of the mobile base from affecting the end-effector control. The overall control framework is illustrated in Figure 3.

2.1. Posture Control in the Null Space

The posture of the redundant robot is controlled in the null space of the task control. In the experimental setup with a mobile manipulator, the task is the motion and force control of the end-effector. The position and orientation of the base is chosen to be the posture coordinates, x_p. Then, the posture dynamics are obtained by projecting eq. (1) into the posture coordinates (Khatib et al. 2004).

$$\Lambda_{p|t}\dot{\vartheta}_p + \mu_{p|t} + p_{p|t} + \bar{J}_{p|t}^T J^T f_c = F_p + \bar{J}_{p|t}^T J^T F, \qquad (8)$$

where

$$\Lambda_{p|t}^{-1} = J_p A^{-1} N^T J_p^T \qquad (9)$$
$$\bar{J}_{p|t}^T = \Lambda_{p|t} J_p A^{-1} \qquad (10)$$
$$\mu_{p|t} = \bar{J}_{p|t}^T b(q,\dot{q}) - \Lambda_{p|t} \dot{J}_p \dot{q} \qquad (11)$$
$$p_{p|t} = \bar{J}_{p|t}^T g(q), \qquad (12)$$

and F is the control force for the task.

The control force, F_p, is composed to compensate the dynamics and the control input for the task.

$$F_p = \hat{\Lambda}_{p|t} f_p^* + \hat{\mu}_{p|t} + \hat{p}_{p|t} + \bar{J}_{p|t}^T J_c^T \hat{f}_c - \bar{J}_{p|t}^T J^T F. \qquad (13)$$

The total torque to be applied to the robot is

$$\Gamma = J^T F + N^T J_p^T F_p. \qquad (14)$$

This results in

$$\dot{\vartheta}_p = f_p^*. \qquad (15)$$

The operational space control structure provides nonlinear dynamic decoupling and dynamic consistency for the task and posture. The task and posture behaviors of the decoupled systems are described in eqs (5) and (15). The control inputs f^* and f_p^* can be designed using a simple PD controller or any other controllers. The stability and performance designed for a given controller at the decoupled system, eq. (5), are achieved at the nonlinear highly coupled system of eq. (2) through the nonlinear dynamic decoupling provided by the control structure of eqs (3) and (4) (Freund 1975; Khatib 1987). Because of the redundancy, the asymptotic stability of the redundant robot (1) requires, in addition, the posture controller of eq. (15) to be asymptotically stable (Khatib 1987). In the next section we present a specific control strategy for the force control portion f_f^* of f^* in eq. (6). The motion control inputs for the task, f_m^*, and posture, f_p^*, will be designed using simple PD controllers.

3. Force Control

The decoupled unit mass system, eq. (5), for each ith translational direction in the operational space coordinate is used for force controller design. The environment in contact is modeled to have a certain stiffness, $k_{s,i}$ (Khatib and Burdick 1986; Figure 4).

$$\dot{f}_{c,i} = k_{s,i} \vartheta_i, \qquad (16)$$

where $f_{c,i}$ is the ith translational direction contact force with the environment. The term ϑ_i denotes the ith translational velocity. With this contact model, the equations of motion of contact force for each translational direction in operational space are,

$$\ddot{f}_{c,i} = k_{s,i} f_i^* \qquad (17)$$

The system transfer function for contact force control in each translational direction is derived from a decoupled subsystem (17). Since the decoupled sub-systems for each translational direction are identical, the sub-script i will be omitted in the following derivations. With an additional damping, $k_v \vartheta$, to f^* for better stability and a system input delay, $T_{i,d}$, the system transfer function, $G(s)$, is

$$G(s) = \frac{k_s e^{-sT_{i,d}}}{s(s+k_v)}, \qquad (18)$$

where k_v is a positive scalar. The discretized state space form of eq. (18) is used for discrete Kalman estimation and control.

$$x_{r,k} = \Phi_r x_{r,k-1} + \Gamma_r u_{k-1}$$
$$y_k = C_r x_{r,k}. \qquad (19)$$

The force control approach in each translational direction is illustrated in Figure 5. The theory of Active Observers (AOBs) is applied to the decoupled linearized second order systems. In AOBs, a Kalman estimator is designed to estimate the states of
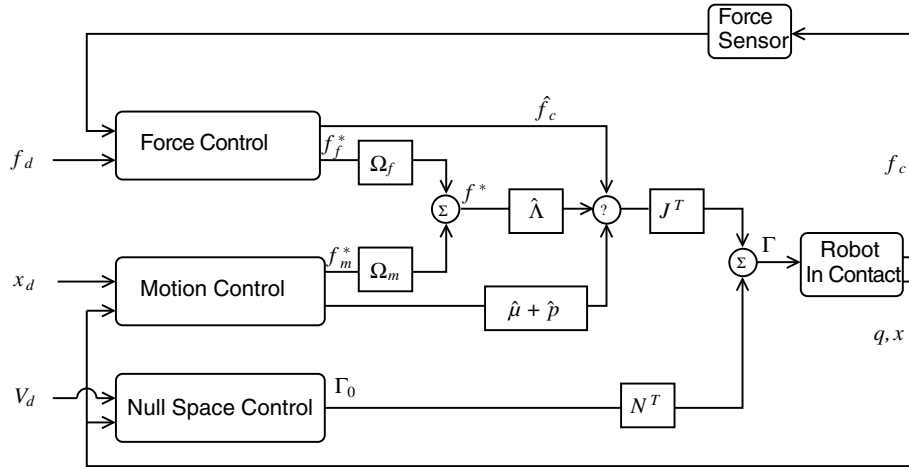
Fig. 3. The motion/force control framework for redundant manipulators. The dynamic decoupling is implemented by compensating for the nonlinear dynamics of the robot such as Λ, μ, and p. The command f^* is composed of the filtered values of motion control, f_m^*, and force control, f_f^*, by the projection matrices, Ω_m and Ω_f. The result of the null space control is pre-multiplied by the projection matrix, N^T, so that it does not disturb the task (motion/force) control.
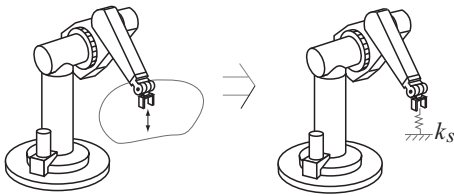

Fig. 4. Spring model of the environment. The contact dynamics of the environment are modeled as a spring with a spring constant of k_s. The illustration shows this model in a vertical direction.

Fig. 5. Force control design. $G(s)$ is the system transfer function from the command f^* to the contact force f_c. f_d is the desired contact force. r_k, $\hat{x}_k$, and $\hat{p}_k$ are reference input, state estimate, and input error estimate. L_r and L_1 are a full state feedback gain and a scaling factor to compute reference input r_k.

the system and the additional state, input disturbance. The estimate of the input disturbance is then directly canceled at the input command (see Figure 5). Full state feedback is applied with the estimated states of the system. The direct cancellation of the estimated input disturbance is an alternative way of implementing integral control.

The AOB method achieves the robust adaptive control in the presence of uncertainties by including input disturbance and process/measurement noise in the estimation (Cortesão 2002). The uncertainties include unmodeled dynamics and imperfect parameter estimations for both the manipulator and the environment. The use of the dynamic equations that do not include the higher order dynamics of the system or nonlinear friction contributes to the modeling errors. Imperfect parameter estimations lead to the imperfect feedback linearization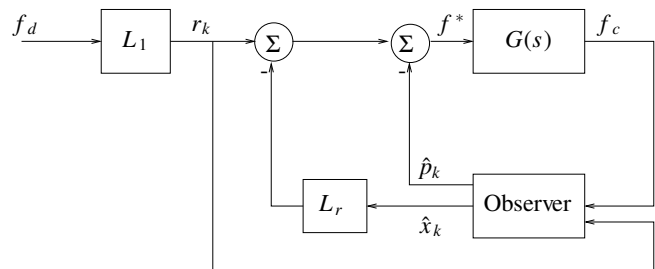 using the operational space formulation. This stochastic estimation strategy provides a way of better estimation of the system states based upon the process noise (modeling uncertainties) and measurement noise. Also, the use of the active state forces the system to follow the desired system response. The most significant uncertainty in the case of the contact force control comes from the incorrect stiffness parameter of the contact environment. The specific robustness analysis with respect to this parameter can be found in Cortesão, Park, and Khatib (2003) while general robustness analysis of AOB method is provided in Cortesão (2002).

Given the input error estimate, p_k, and allowing the process/measurement noise, we have

$$x_{a,k} = \Phi_a x_{a,k-1} + \Gamma_a u_{k-1} + \xi_k$$
$$y_k = C_a x_{a,k} + \eta_k, \tag{20}$$

where

$$x_{a,k} = \begin{bmatrix} x_{r,k} \\ p_k \end{bmatrix} \quad , \quad \Phi_a = \begin{bmatrix} \Phi_r & \Gamma_r \\ 0 & 1 \end{bmatrix}$$

$$\Gamma_a = \begin{bmatrix} \Gamma_r \\ 0 \end{bmatrix} \quad , \quad C_a = [C_r \quad 0] \tag{21}$$

and the stochastic inputs ξ_k and η_k are model and measurement uncertainties.

A full state feedback gain, L_r is designed using a pole placement method (Ackermann's formula; Franklin, Powell, and Emami-Naeini 2002). Combining the state feedback with the direct compensation of the input error estimate, the input to the system is

$$u_{k-1} = r_{k-1} - L_a \hat{x}_{a,k}$$
$$L_a = [L_r \quad 1]. \tag{22}$$

The state estimation is based on (20) and (22).

$$\hat{x}_{a,k} = \hat{x}_{a,k|(k-1)} + K_k(y_k - \hat{y}_k) \tag{23}$$
$$\hat{x}_{a,k|(k-1)} = \Phi_{a,closed} \hat{x}_{a,k-1} + \Gamma_a r_{k-1} \tag{24}$$
$$\Phi_{a,closed} = \begin{bmatrix} \Phi_r - \Gamma_r L_r & 0 \\ 0 & 1 \end{bmatrix} \tag{25}$$
$$\hat{y}_k = C_a \hat{x}_{a,k|(k-1)} \tag{26}$$

The Kalman gain K_k is

$$K_k = P_{1k} C_a^T [C_a P_{1k} C_a^T + R_k]^{-1} \tag{27}$$

with

$$P_{1k} = \Phi_a P_{k-1} \Phi_a^T + Q_k$$
$$P_k = P_{1k} - K_k C_a P_{1k}. \tag{28}$$

The term Q_k is the system noise matrix representing model uncertainty, R_k is the measurement noise variance matrix, and P_k is the mean square error matrix of the states. More details on this implementation and robust analysis can be found in Cortesão, Park, and Khatib (2003).

3.1. Stiffness Adaptation

The slave manipulator in teleoperation experiences contact with different environments. The knowledge of the stiffness, k_s, is important not only for force control but also for modifying the virtual spring, k_{vir}, in order to provide better telepresence to the operator. The changes in the environment's stiffness can be abrupt and large in magnitude. Although the contact force controller designed with AOB is robust to the change of environmental stiffness, its performance will degrade when there is a mismatch between estimated and actual stiffness and the system might be unstable if the mismatch is beyond the stability margin. These are demonstrated in the experiments in the presence of a large mismatch of the environment stiffness, as shown in Figure 6. Thus, a fast on-line stiffness estimation strategy is required to cope with these changes.

A review of estimation methods for contact stiffness and damping is presented in Erickson, Weber, and Sharf (2003). A signal processing method, an indirect adaptive controller (Seraji and Colbaugh 1997), a model reference adaptive controller (Singh and Popa 1995), and a recursive least-squares estimation technique (Love and Book 1995) are reviewed. The signal processing method requires off-line implementation while the other three methods are implemented on-line. However, these on-line methods still require exciting signals over time to compute the model parameters. These algorithms are based on quantities such as the measured contact force and deflected position. Although these approaches have demonstrated convergence between estimated and actual stiffness, the time required to achieve this convergence increases as the robot's motion slows or when the motion is less than the resolution of the encoders. This situation often occurs in haptic teleoperation when the robot touches a rigid surface or is stationary in free space. Therefore, although stiffness identification is accomplished, the performance of the control is severely degraded prior to convergence of the estimated stiffness.

While the stiffness estimation methods reviewed in Erickson, Weber, and Sharf (2003) seek to accurately estimate stiffness, in haptic teleoperation obtaining a highly accurate estimate of the stiffness is not as critical as achieving consistent performance at all times. Therefore, a different estimation approach is sought which satisfies the specific requirements for haptic teleoperation.

An approach for stiffness estimation in a haptically teleoperated system will be presented. The basis for the stiffness adaptation law used in this approach is derived from the fact that the responses of the measured and estimated contact forces are correlated to the stiffness modeling errors. Large deviations between the measured and estimated force responses indicate that the stiffness modeling error is larger than expected.

The different relationships between the desired, measured, and estimated contact force (f_d, f_m, and f_e), shown in Figure 6(a) and (b), are noticeable. The estimated or nominal stiffness $\hat{k}_s$ is used in the design of full state feedback and the Kalman estimator. Figure 6(a) shows the results when $k_s \gg \hat{k}_s$. The high deviation of contact force in a short time period occurs due to the under-estimation of stiffness. Because the controller perceives the environment to be more compliant than it actually is high feedback gains are chosen to control the contact force. Therefore, in this case, the controller
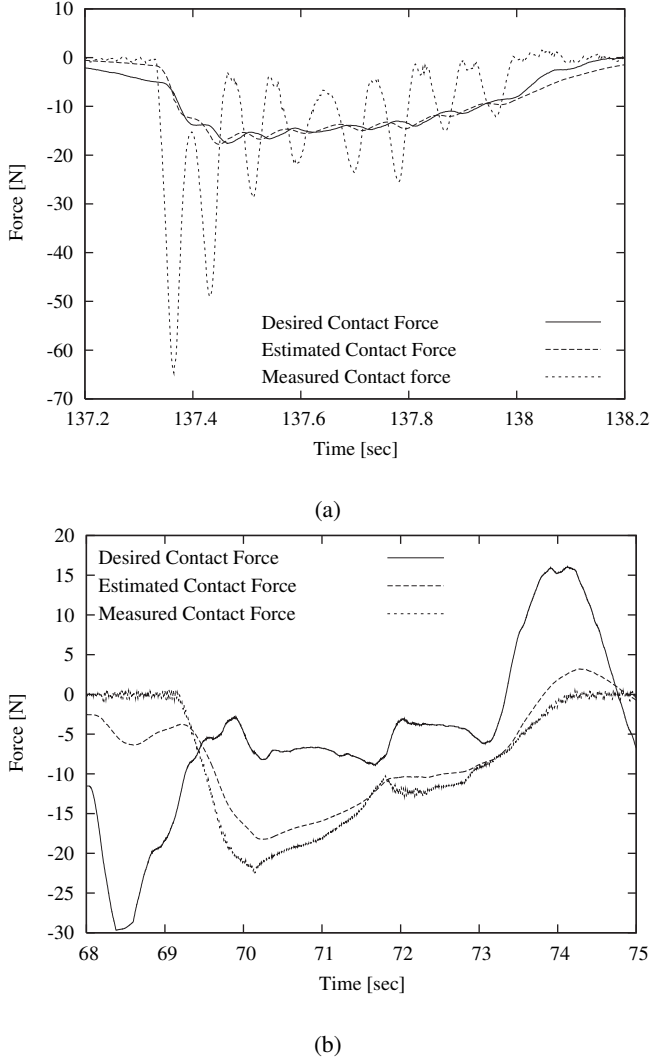
(a)

(b)

Fig. 6. The results of force control without adaptation. (a) Nominal stiffness, $\hat{k}_s$, is 100 N/m and k_s changes from free space to 6000 N/m. (b) Nominal stiffness, $\hat{k}_s$ is 3000 N/m and k_s changes from free space to 300 N/m.

over-compensates for the errors, resulting in under-damped responses. Eventually instability could arise if the stiffness mismatch becomes too large.

In contrast, Figure 6(b) demonstrates the typical results when $k_s \ll \hat{k}_s$. In this case, the full state feedback gains are too small due to the over-estimation of stiffness. This results in under-compensation for errors and a sluggish response.

We notice that the measured and estimated contact forces in the first case ($k_s \gg \hat{k}_s$) are oscillatory in a very short time period. The estimated contact forces from the Kalman estimator are computed based on the weighting between two stochastic parameter matrices (measurement and processing noise uncertainties). The oscillatory response of the measurement in

the first case causes the estimated values to be closer to the desired values than to the measured values. This is because the measurement updates in the Kalman estimator are unable to track the rapid changes in the measured value. Thus the estimate tends to average out over the measurement oscillations. In the second case ($k_s \ll \hat{k}_s$) we notice that the estimated contact force tracks the measured contact force reasonably well but that the desired contact force is not tracked well because of the low gain response of the controller. Figure 7 illustrates the differences between these two cases. It is observed that the difference between f_m and f_e is larger than the difference between f_d and f_e when $k_s \gg \hat{k}_s$. Conversely, the difference between f_d and f_e is larger than the difference between f_m and f_e when $k_s \ll \hat{k}_s$. The first part of the stiffness adaptation law is motivated by these very different response characteristics. The second part of the adaptation law is motivated by the fact that the system stiffness increases when larger contact force is applied.

The stiffness adaptation law combines these two aforementioned ideas.

$$\hat{k}_s^i = \hat{k}_{s,1}^{f,i} + \hat{k}_{s,2}^{f,i}. \tag{29}$$

where the superscript i indicates the discrete time step and the superscript f indicates the filtered value. The first part of the estimation is based upon the relation between f_d, f_m, and f_e.

$$\hat{k}_{s,1}^i = \hat{k}_{s,1}^{i-1} + \Delta \hat{k}_{s,1}^i, \tag{30}$$

where

$$\begin{aligned} \Delta \hat{k}_{s,1}^i = & k_1 |f_m - f_e| \, \sigma_d \left(c, \frac{|f_m - f_e|}{|f_e| + a_1} - b_1 \right) \\ & - k_2 |f_d - f_e| \, \sigma_d \left(c, \frac{|f_d - f_e|}{|f_e| + a_2} - b_2 \right), \end{aligned} \tag{31}$$

and

$$\sigma_d(c, x) = \frac{1}{1 + e^{-cx}}. \tag{32}$$

The terms k_1, k_2, a_1, a_2, b_1, b_2 and c are positive parameters. The minimum of $\hat{K}_{s,1}$ is kept to 0 N/m. The second part of the estimation law (29) is based on the fact that the stiffness increases with the applied force.

$$\hat{k}_{s,2} = k_{min} + k_3 \, \sigma_d \left(c_0, |f_m| - f_0 \right), \tag{33}$$

where f_0, c_0 and k_3 are positive parameters. k_{min} is set to 100.0 N/m in the experiments. Finally, low-pass filters are used to prevent jerking motions due to quick changes in the stiffness estimation. All the parameters are obtained experimentally: a_1, a_2, b_1, b_2, c, and c_0 are 1.0, 0.1, 1.5, 1.0, 5.0, and 0.2 respectively. f_0, k_1, k_2, and k_3 are 20 N, 10 m^{-1}, 10 m^{-1}, and 3000 N/m respectively.

The adaptation heuristic has been designed from the experimental data by trial and error. The robustness and effectiveness have been verified through numerous experiments. Stability of the system with this adaptation is guaranteed since the
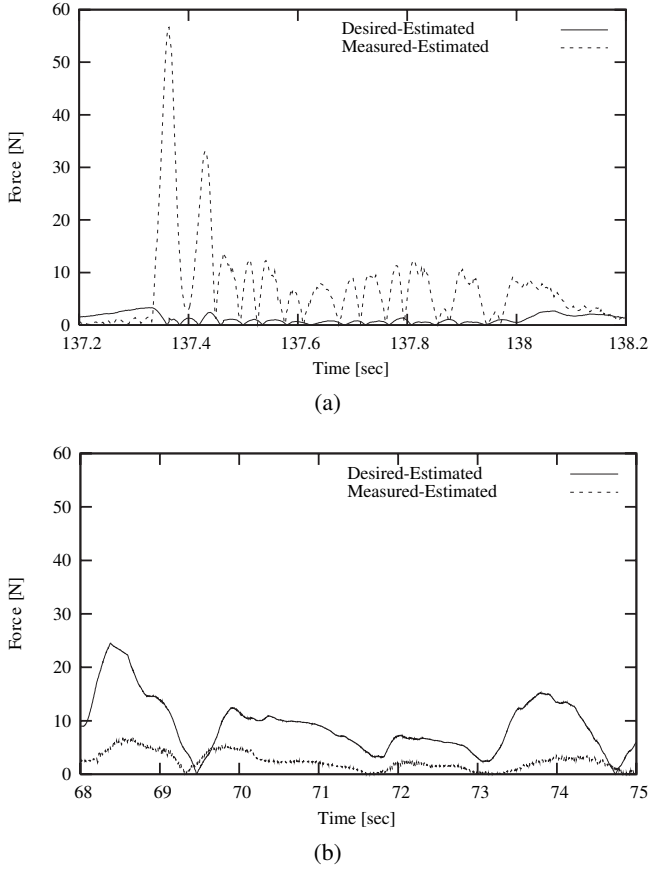
(a)

(b)

Fig. 7. Comparison among the desired, estimated, and measured contact forces in the case of force control without adaptation. (a) Nominal stiffness, $\hat{k}_s$, is 100 N/m and k_s changes from free space to 6000 N/m. (b) Nominal stiffness, $\hat{k}_s$ is 3000 N/m and k_s changes from free space to 300 N/m.

proposed adaptation increases the stiffness estimation whenever it shows the underdamped response. This lowers the control feedback gains such that the system is stabilized. Since this adaptation law is designed and adjusted for the specific experimental setup, a more general automatic procedure, such as neural networks or learning techniques, would be useful in applications to other systems. The successful implementation of this adaptation law shows great potential for refinement using advanced learning/adaptive techniques.

4. Teleoperation

The teleoperation approach is developed for each direction in the operational space coordinate (i.e., one DOF system) since the control structure in Section 2 enables each of the task coordinates of a manipulator end-effector to be controlled

independently. Figure 8 illustrates the proposed teleoperation approach where the master and slave systems are connected by a virtual spring. Force control is then used on the slave manipulator to eliminate the dynamics of the slave robot.

The desired force, f_d, for both master and slave systems is generated by the virtual spring k_{vir} due to the position difference. The contact force on the slave end-effector is controlled to track the desired force, f_d. The force controller in the slave system is implemented using a modified Kalman Estimator with full state feedback (AOB). However, only feedforward control is used to generate the desired force on the master side since the device is light weight and has low friction.

Stability characteristics of the system are improved by providing the desired contact force to the operator rather than the measured contact force. The direct use of the measured contact force causes a delay in the loop and the stability of the system is greatly dependent upon the mass ratio of the master and slave systems (Daniel and McAree 1998).

4.1. Telepresence

The user is always provided with the contact force that is scaled by s_f through a haptic device if the force control in the slave robot tracks the desired contact force well. Moreover, the transfer function, $\frac{X_m(s)}{F_h(s)}$, from the force of a human operator to the master position represents the compliance that the human operator feels at the master device (Lawrence 1993). Telepresence would be realized if the transfer function closely matches the contact compliance on the slave system.

In Figure 8, the master device is modeled with a mass and damper system, having the transfer function of $1/(m_m s^2 + c_m s)$. The slave system represents the force controlled robot in contact with environment. Thus, the transfer function from the desired force to the slave position, $\frac{X_s(s)}{F_d(s)}$, is represented by $G_{se}(s)$. The equations of motion for the master and slave are

$$(m_m s^2 + c_m s)X_m(s) = \\ F_h(s) - s_f k_{vir}\{s_p X_m(s) - X_s(s)\} \qquad (34)$$

$$G_{se}(s)k_{vir}\{s_p X_m(s) - X_s(s)\} = X_s(s), \qquad (35)$$

where $X_m(s)$ and $X_s(s)$ are the Laplace Transform of x_m and x_s. Moreover, the environment in contact is modeled to have a certain stiffness, k_s, in eq. (16),

$$f_c = k_s x_s, \qquad (36)$$

where f_c is the contact force with the environment. Therefore, $G_{se}(s)$ can be represented by

$$G_{se}(s) = \frac{X_s(s)}{F_d(s)} = \frac{1}{k_s}\frac{F_c(s)}{F_d(s)}. \qquad (37)$$

$G_s(s) = \frac{F_c(s)}{F_d(s)}$ is the closed loop transfer function of the force controller in the slave system; thus, $G_{se}(s) \approx \frac{1}{k_s}$ within the
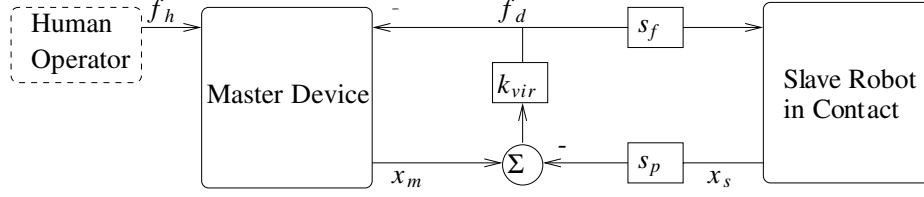
Fig. 8. Teleoperation Scheme. x_m, x_s, s_p and s_f are the master position, slave position, position scaling and force scaling, respectively. s_p and s_f are 2.0 and 0.1 in the experimental setup. k_{vir} is the virtual spring that generates the desired force, f_d.

bandwidth of the force controller. From (34) and (35), the transfer function $\frac{X_m(s)}{F_h(s)}$ can be derived as

$$\frac{X_m(s)}{F_h(s)} = \frac{k_{vir} + G_{se}^{-1}(s)}{\Delta}, \tag{38}$$

where

$$\Delta = (m_m s^2 + c_m s + k_{vir} s_p s_f)(k_{vir} + G_{se}^{-1}(s)) \\ - k_{vir}^2 s_p s_f. \tag{39}$$

Equation (38) shows the characteristics of the proposed teleoperation approach. If $k_{vir} \gg |G_{se}^{-1}|$, at a low frequency range, $|m_m s^2 + c_m s| \ll k_{vir} s_p s_f$, the compliance that a human operator feels will be close to the environment compliance, $\frac{X_m(s)}{F_h(s)} \approx \frac{1}{s_p s_f k_s}$. At a high frequency range, $|m_m s^2 + c_m s| \gg k_{vir} s_p s_f$, it will be $\frac{X_m(s)}{F_h(s)} \approx \frac{1}{m_m s^2 + c_m s}$. Therefore, the key aspect for telepresence is to maintain $k_{vir} \gg |G_{se}^{-1}|$, i.e., $k_{vir} \gg k_s$, in addition to having a large force control bandwidth. The value of k_{vir} is limited by the stability. To maintain the ratio $\frac{k_{vir}}{k_s}$ as large as possible within this limit, k_{vir} is updated on-line based upon the estimated environment stiffness. That is, k_{vir} is increased with the estimate of k_s. The following equation is used in the experiments (Figure 9).

$$k_{vir} = 2000.0 \sigma_d(0.007(\hat{k}_s - 1000.0)) + 1000.0 \tag{40}$$

where $\sigma_d(x) = \frac{1}{1+e^{-x}}$.

4.2. Stability

The characteristic equation Δ of the loop is

$$\Delta = (m_m s^2 + c_m s)G_{se}(s)^{-1} \\ + k_{vir}(m_m s^2 + c_m s + s_p s_f G_{se}(s)^{-1}). \tag{41}$$

The system is stable for any k_{vir} if the model is perfect because $G_{se}(s)$ is a stable minimum phase system with a constant DC value. However, the feedback gains k_{vir} and k_{vir}/k_s are bounded by the physical limitations of the master device and the slave robot. Figure 10 shows the local feedback systems at the master and slave. Specifically, k_{vir} cannot exceed the maximum stiffness that the master device can produce.

Also, $\frac{k_{vir}}{k_s}$ is limited by the motion bandwidth of the slave manipulator. In free space motion, where k_s is small, this results in greater limitation on the magnitude of k_{vir}.

4.3. Time Delay

The block diagram in the presence of time delay is shown in Figure 11. Accounting for the time delay, eqs (34) and (35) become

$$(m_m s^2 + c_m s)X_m(s) = F_h(s) - s_f k_{vir}\{s_p X_m(s) \\ - X_s(s)e^{-T_d s}\} \tag{42}$$

$$G_{se}(s)k_{vir}\{s_p X_m(s)e^{-T_d s} - X_s(s)\} = X_s(s) \tag{43}$$

Now, the transfer function from the force of the human operator to the position of the master device is

$$\frac{X_m(s)}{F_h(s)} = \frac{k_{vir} + G_{se}^{-1}}{\Delta'}, \tag{44}$$

where

$$\Delta' = (m_m s^2 + c_m s + k_{vir} s_p s_f)(k_{vir} + G_{se}^{-1}) \\ - k_{vir}^2 s_p s_f e^{-2T_d s}. \tag{45}$$

The stability of the system is no longer guaranteed due to the communication delay, T_d. Nyquist stability criteria (Franklin, Powell, and Emami-Naeini 2002) can be used to investigate the characteristic equation Δ' in eq. (45) for the stability margin due to the time delay. The Nyquist stability analysis has been conducted for our current master and slave system. The physical parameters of the master device, Phantom 1.0 from SensAble Technologies, are refered in Diolaiti et al. (2005). The stability margin of the experimental system is identified as approximately 52 ms for the round-trip time delay.

The effect of time delay on the performance is investigated using Padé approximation for small time delay, $e^{-2T_d s} = \frac{1-T_d s}{1+T_d s}$.

$$\left[\frac{F_h(s)}{X_m(s)}\right]_{\text{w delay}} = \left[\frac{F_h(s)}{X_m(s)}\right]_{\text{w/o delay}} + \frac{k_{vir}^2 s_p s_f \frac{2T_d s}{1+T_d s}}{k_{vir} + G_{se}(s)^{-1}} \tag{46}$$

The additional term, $\frac{k_{vir}^2 s_p s_f \frac{2T_d s}{1+T_d s}}{k_{vir} + G_{se}(s)^{-1}}$, can be further approximated as $2s T_d k_{vir} s_p s_f$ at a low frequency range when $k_{vir} \gg |G_{se}^{-1}|$. This shows the damping effect of the time delay.
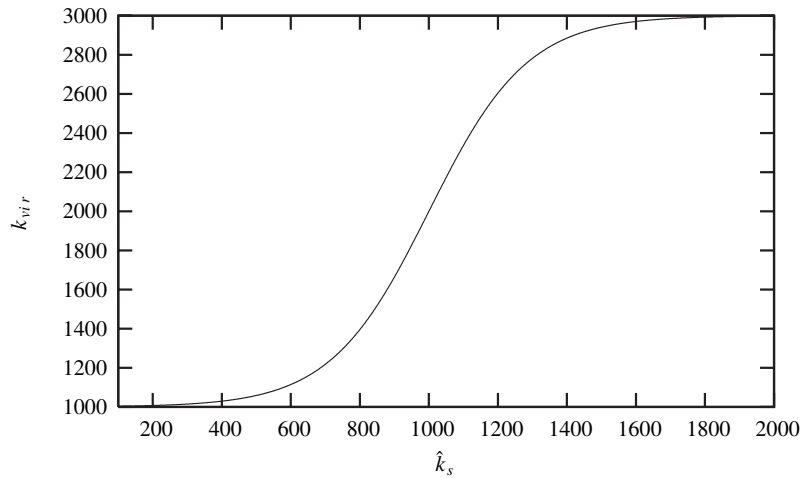
Fig. 9. Updates of k_{vir} with the estimate of k_s. $\hat{k}_s$ is the estimate of the environment stiffness k_s.
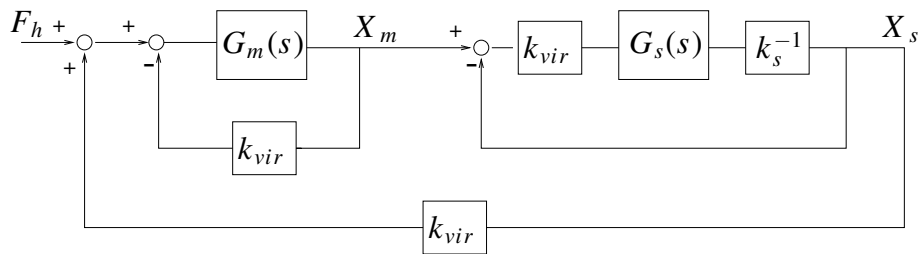

Fig. 10. Re-arranged block diagram. It highlights local feedback for each system in the proposed teleoperation scheme. $G_m(s)$ and $G_s(s)$ represent dynamics of the master device and the closed loop force control system of the slave manipulator. i.e., $G_m(s) = \frac{X_m(s)}{F(s)} = (m_m s^2 + c_m s)^{-1}$ and $G_s(s) = \frac{F_c(s)}{F_d(s)}$. X_m and X_s are the position of the master and slave system. F_h is the force from a human operator. F_c and F_d are the contact force and the desired contact force in the slave manipulator. k_s is the environment stiffness.

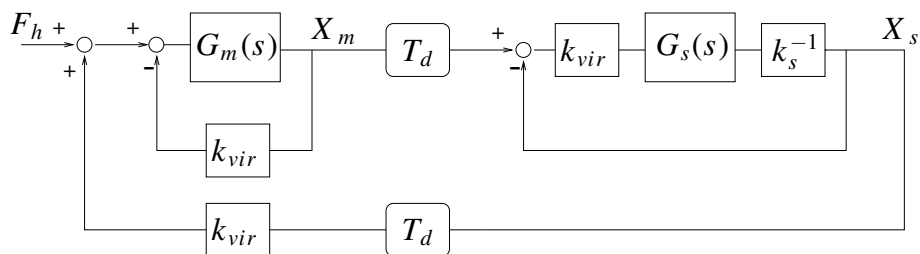
Fig. 11. Re-arranged block diagram with communication time delay. The communication time delay, T_d, is added to the block diagram in Figure 10.

5. Experimental Setup

The slave station consists of a PUMA560 manipulator mounted on an XR4000 mobile base. The PUMA560 robot is controlled through TRC205 amplifier package from Mark V Automation Corporation. This amplifier package is connected to a PC running a QNX real-time operating system. The servo program in QNX commands torques to the robot through this setup. The XR4000 mobile base is from Nomadic Technologies. The nomadic XR4000 mobile base is a holonomic robotic vehicle which has 4 powered casters. The driver for the XR4000 implemented in QNX takes as input two translational forces and one torque about the vertical axis. Thus, the robot is treated as having two prismatic joints and one revolute joint (Holmberg and Khatib 2000). The servo rate is 500 Hz and the computed torque is commanded to the slave mobile robot (PUMA560 and XR4000) at the end of each servo loop. The dynamic model and inertial parameters of the PUMA560 robot are in Armstrong, Khatib, and Burdick (1986).

PHANTOM 1.0A from SensAble technologies is used for the master device. The haptic device is running on a PC with a LINUX operating system. Since it is not running on a real-time operating system, the servo rate slightly varies. An average servo rate is about 10 000 Hz. The communication between the master and slave systems uses a wireless LAN network. The round-trip communication delay between the servo programs for the PUMA560 and the PHANTOM device is about 52 ms.

Throughout the experiments, the translational directions of the end-effector are controlled by teleoperation through force control. The end-effector orientation is controlled to maintain a fixed orientation. Either direct vision or indirect vision through a video is provided to the user at the master device. In the case of video visual feedback, the feedback latency is negligibly small. The teleoperation system is intuitive to operators. So, it does not require any training to operate the system. The experimental data to be presented in the next section is a typical result, which was gathered by a single operator. Further testing is needed to determine how effectively realistic teleoperation tasks can be conducted with trained and naive operators.

6. Results

Two sets of experiments were conducted to demonstrate the decoupling of the end-effector control from the base control. Only the PUMA robot was controlled in the first set of experiments while both the PUMA robot and the base were controlled in the second experiments. The experimental results from the first experiments are shown in Figures 13 and 14. The second set of experiments was conducted while the base was controlled to move in the lateral direction (i.e., along the table in Figure 12) using null space control. The desired trajectory was a sine function with an amplitude of 20 cm and a period of 12 seconds as shown in Figure 16(d). The results

(a)
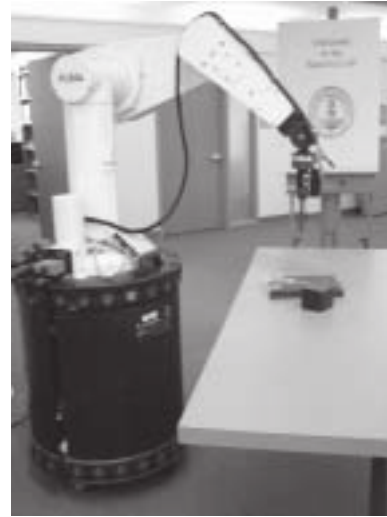
(b)

Fig. 12. System Setup. (a) Phantom™ device controlled by a human. (b) PUMA robot mounted on XR4000 (ROMEO).

are shown in Figures 15 and 16. The consistent performance of the two sets of experiments demonstrates the effectiveness of the decoupled control structure.

In both experiments, the operator began moving the slave manipulator in free space (i.e., no contact) by teleoperation. Different objects were then contacted sequentially by the end-effector of the slave manipulator. These included a sponge, a book, and a table. The robot was in free space in between the contacts (i.e., where $f_m \approx 0$). The operator was asked to contact different objects with the same amount of force. The stiffness of the sponge and the book were computed off-line using the measured contact force and contact position. These were approximately 300 and 6000 N/m at low values of contact forces (up to about 20 N)[1]. The table in the experiments is composed of aluminum plates and frames. The off-line computation of its stiffness is limited due to the resolution of the end-effector position measurement. Based upon the material

---

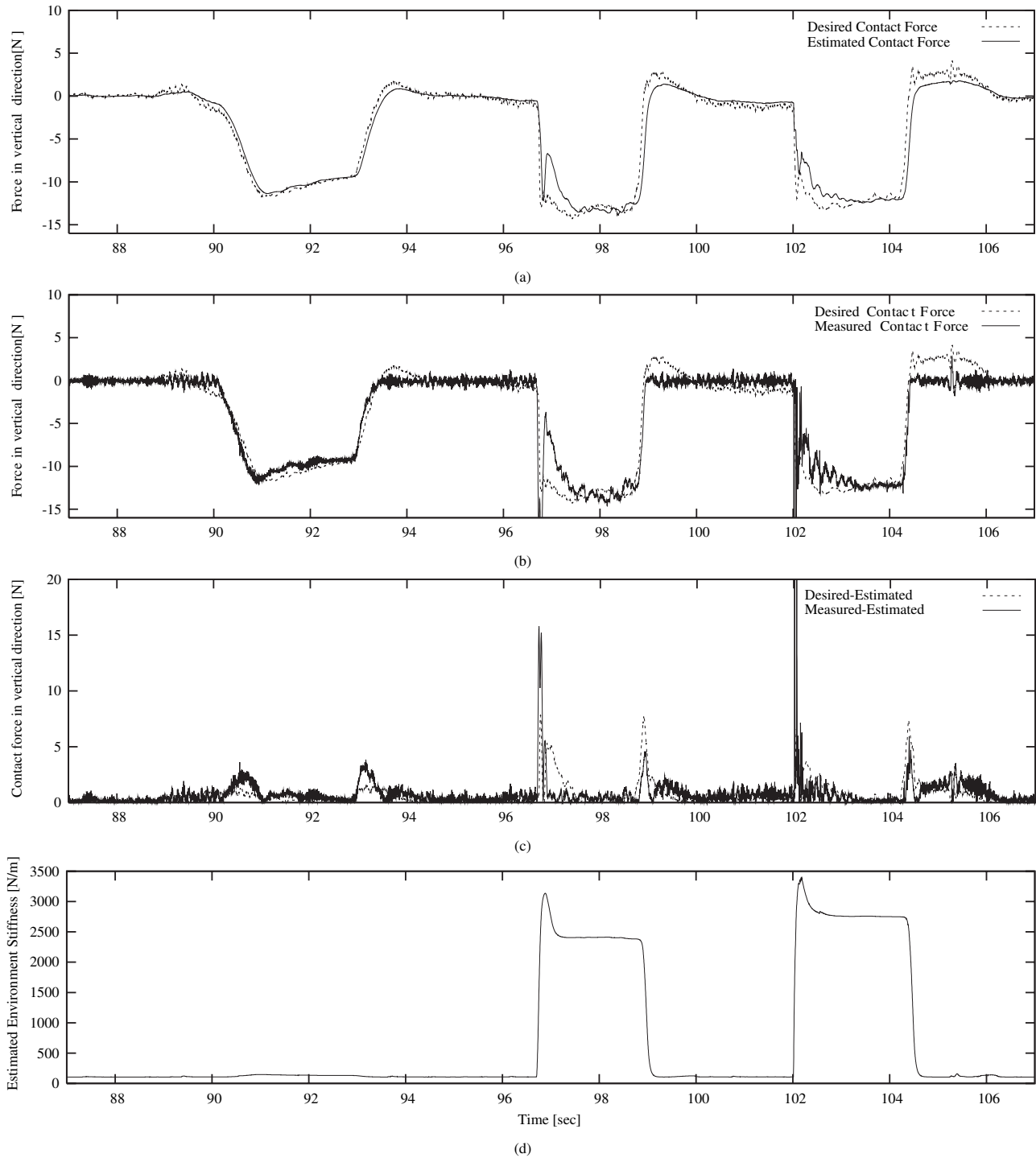1. However, the stiffnesses of them increase as larger forces are applied.

Fig. 13. Fixed base teleoperation: results of contact force control. Teleoperation began when the slave manipulator was in free space. Only the PUMA was used as the slave robot. Different objects were then contacted sequentially by the slave robot: a sponge, a book, and a table. The robot was in free space in between the contacts. The desired, estimated, and measured force at the end-effector of the slave manipulator are compared in (a) and (b). The desired force is generated by a virtual spring, $k_{vir}(x_m - x_s)$. The estimated force is from the AOB (a modified Kalman Estimator). The force is measured by the JR3 wrist force sensor. The peaks of the measured contact force at 96.7 s and 102 s in (b) reaches to -22 N and -82 N, respectively. The plot in (c) compares the difference between the desired and the estimated contact forces with the difference between the measured and estimated contact forces. This demonstrates the effectiveness of the stiffness estimation compared with Figure 7. The peak of the difference between the measured and estimated contact force at 102 s reaches to 80 N. The result of on-line stiffness estimation is plotted in (d).
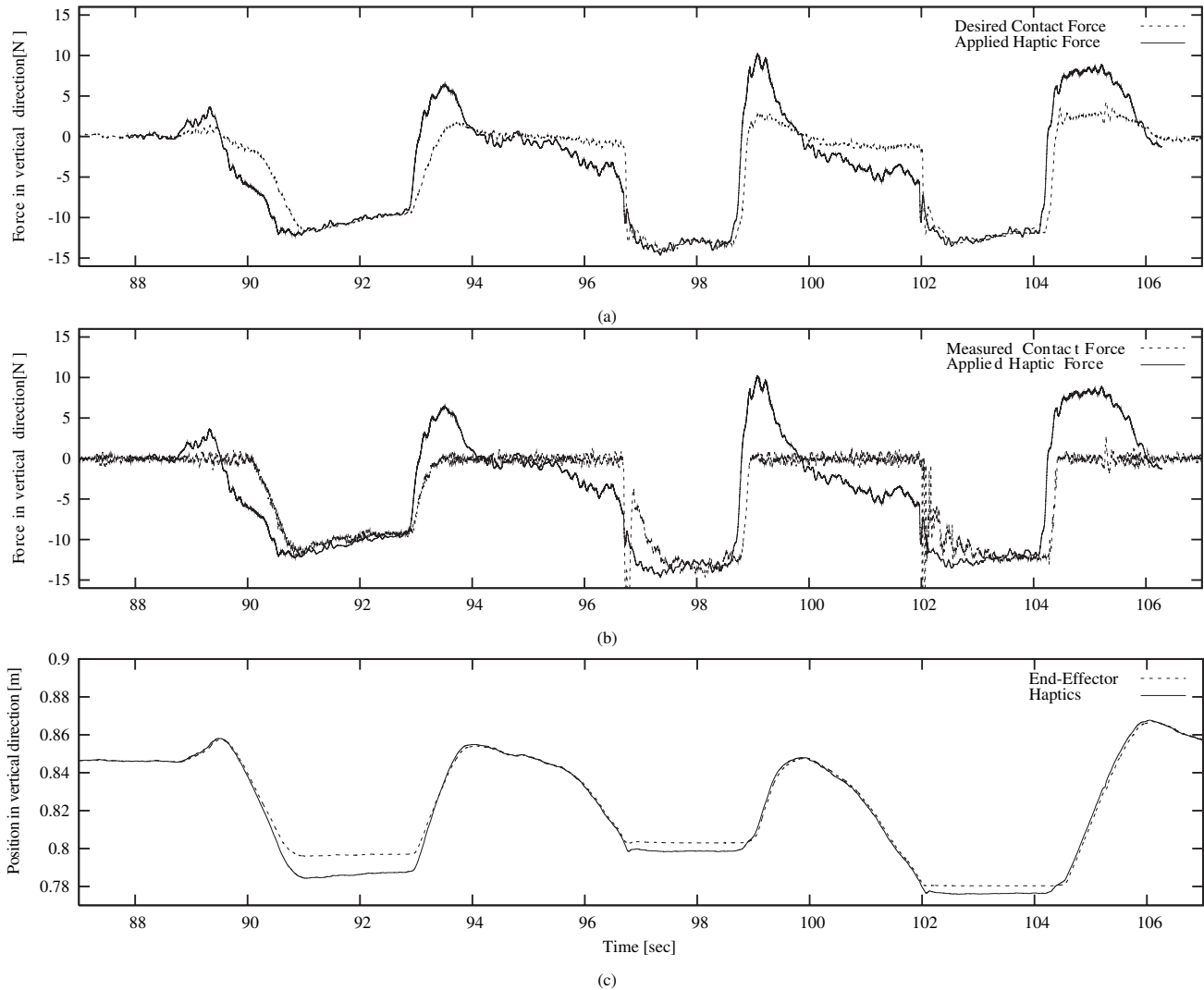
Fig. 14. Fixed base teleoperation: force feedback to user and position tracking. The data plots are for the same experiments as in Figure 13. Applied haptic force at the master device is compared with the desired and measured contact forces at the slave robot in (a) and (b). The haptic force is multiplied by the force scaling factor, 10.0, for comparison. The peaks of the measured contact force at 96.7 s and 102 s in (b) reaches to -22 N and -82 N, respectively. The difference between the applied haptic force and desired contact force in (a) is due to the communication time delay. They must have been identical in the case of no time delay. The plot in (c) shows the tracking of the position of the slave robot end-effector to the haptic device position.
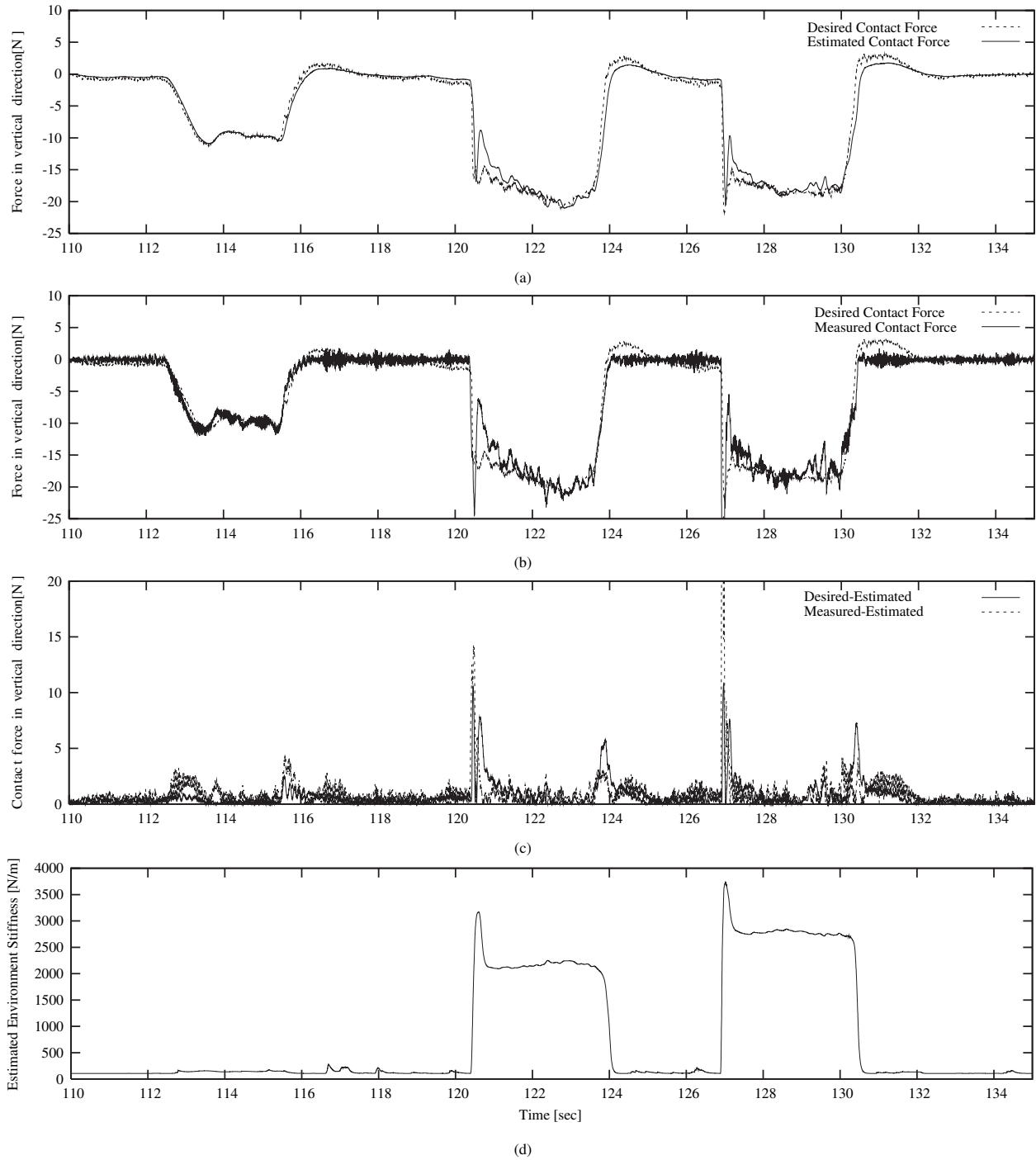
Fig. 15. Moving base teleoperation: results of contact force control. Teleoperation began when the slave manipulator was in free space. The slave manipulator was composed of Both the PUMA and XR4000 mobile base. Different objects were then contacted sequentially by the slave robot: a sponge, a book, and a table. The robot was in free space in between the contacts. The desired, estimated, and measured force at the end-effector of the slave manipulator are compared in (a) and (b). The desired force is generated by a virtual spring, $k_{vir}(x_m - x_s)$. The estimated force is from the AOB (a modified Kalman Estimator). The force is measured by the JR3 wrist force sensor. The peak of the measured contact force at 126 s in (b) reaches to -43 N. The plot in (c) compares the difference between the desired and the estimated contact forces with the difference between the measured and estimated contact forces. This demonstrates the effectiveness of the stiffness estimation compared with Figure 7. The peak of the difference between the measured and estimated contact force at 127 s reaches to 37 N. The result of on-line stiffness estimation is plotted in (d).
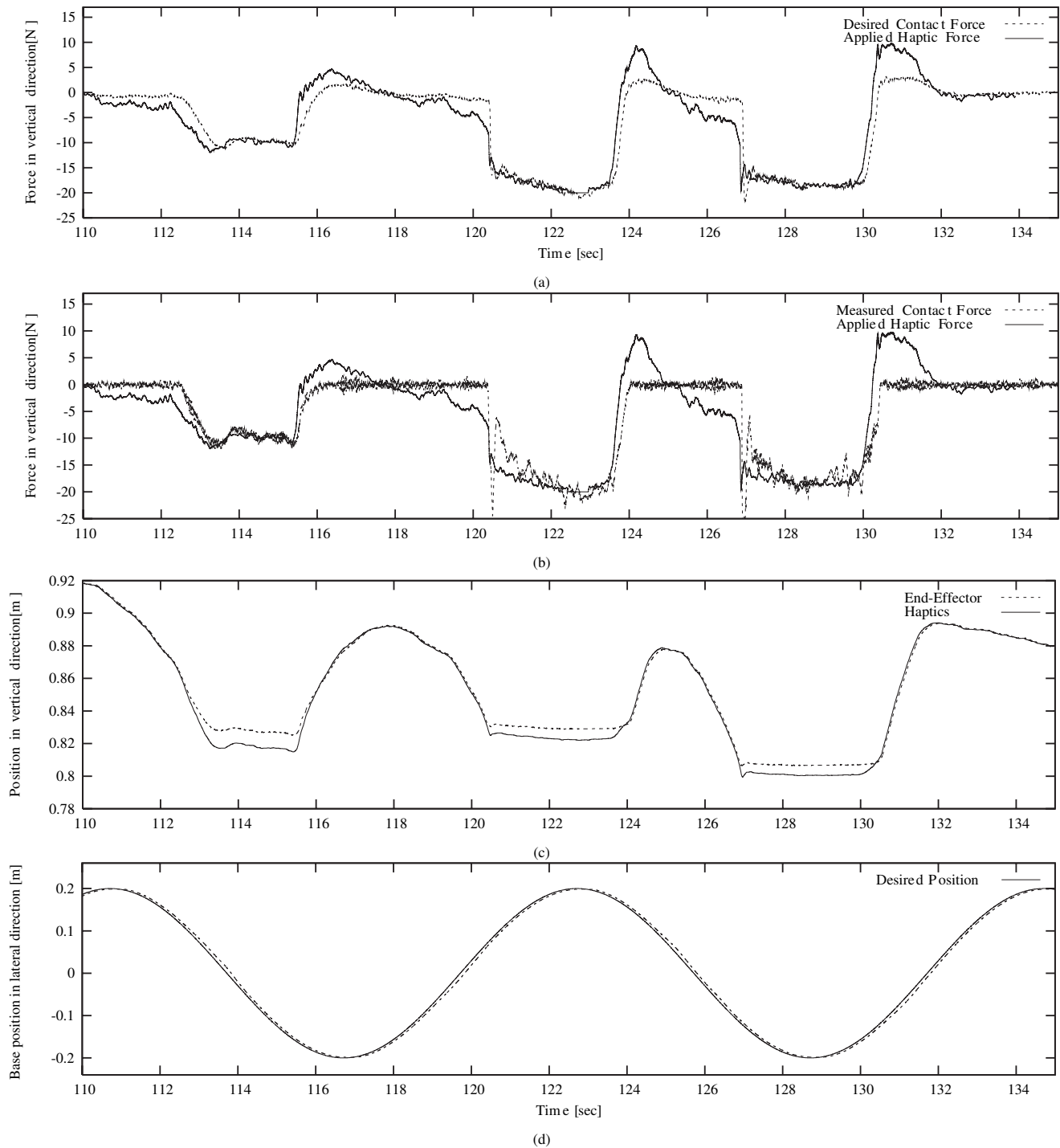
Fig. 16. Moving base teleoperation: force feedback to user and position tracking. The data plots are for the same experiments as in Figure 15. Applied haptic force at the master device is compared with the desired and measured contact forces at the slave robot in (a) and (b). The haptic force is multiplied by the force scaling factor, 10.0, for comparison. The peak of the measured contact force at 126 s in (b) reaches to -43 N. The difference between the applied haptic force and desired contact force in (a) is due to the communication time delay. They must have been identical in the case of no time delay. The plot in (c) shows the tracking of the position of the slave robot end-effector to the haptic device position.

properties and the geometry of the table[2], the stiffness has been computed to be approximately 50 000 N/m. Figures 13 and 15 show the results of the contact force controller and stiffness estimation in the vertical direction on the slave manipulator. The manipulator was in free space in the region where the measured contact forces were near zero. The results demonstrate that the force controller with AOBs and stiffness adaptation performs well even in the presence of vastly different environmental changes. Although the actual stiffness changed from free space to 300, 6000, and 50 000 N/m, the estimated environment stiffness $\hat{k}_s$ was updated quickly enough to achieve the designed performance. The effectiveness of the stiffness adaptation can be observed by comparing Figures 13(c) and 15(c) with Figure 7. The differences among the desired, measured, and estimated forces have been significantly reduced by effective adaptation to the different environments.

It is noted that the stable transition from free space to the three surfaces were achieved. The velocities of the end-effector were approximately 5 cm/s at the impacts to all three environments (Figures 14(d) and 16(d)). Especially, the stability was maintained during the transition to rigid surfaces (the book and the table). The updates of the stiffness in hard contact were within 0.1 s. The stability of the contact force control in transition was realized by effective stiffness adaptation and robust contact force control.

The applied haptic forces are compared with the desired contact forces of the slave end-effector in Figures 14(a) and 16(a). The difference between the applied haptic force and the desired contact force of the slave robot illustrates the effect of communication delay of the system. The difference would be zero if there were no communication delay. However, the effect of time-delay results in large differences especially in free space motion. This contributes to the damping effect that the user feels, which is discussed in Section 4.3. Figures 14(b) and 16(b) compare the measured contact force with the applied haptic force to the operator. These plots show how close the contact force measurement and the haptic feedback to the user are. The results show that the force feedback to the user closely matches the measured contact force in contact. However, the user feels damping effect in free space motion.

Figures 14(c) and 16(c) show position tracking performance. It is noted that the positions of the haptic device and the robot end-effector successfully follow each other in the free space motion. In contact, the virtual spring generates the desired contact force for both master and slave robots based upon the difference between the master and slave positions.

A multimedia extension 1 contains a video clip showing a demonstration of a teleoperated mobile manipulator *setting a dinner table*. An operator controls the translational directions of the end-effector through teleoperation to set a dinner table.

The mobile base is autonomously controlled to keep a certain distance from the table and follow the end-effector along the table. The orientation of the end-effector is commanded to move to specific orientations by the keyboard strokes of the operator.

7. Conclusion

The integration of contact force control with stiffness adaptation and a virtual spring provides a modular and systematic control structure for teleoperation. The translational motion of the robot is always controlled by the contact force control without any discrete switching by using on-line stiffness estimation. In the case of no contact it is assumed that the robot is in a very compliant contact.

Active force control enables the overall teleoperation approach to have the robustness and performance needed for providing force feedback to a human operator. The bandwidth of the active force control determines how realistic the force feedback is. Transitions between environments with various stiffnesses do not involve any switching in the control structure, as the on-line stiffness adaptation performs effectively to match large changes in the environment. Stability margin due to the transmission time delay is analyzed. The implementation on the experimental setup demonstrated that the system is stable in the presence of 52 ms round-trip communication delay. The experimental results on the mobile platform demonstrated that the proposed teleoperation approach fits within the operational space formulation. In this way, the user only controls the translational motion of the end-effector through teleoperation, while the other DOF are autonomously controlled without disturbing the task.

Appendix: Index to Multimedia Extensions

The multimedia extension page is found at http://www.ijrr.org.

Table of Multimedia Extensions

Extension	Type	Description
1	Video	Haptic teleoperation — setting a dinner table

---

2. A table with PB (Particle-Board) wood was also used in the experiments. Although the stiffness of the PB wood plate is harder than that of the aluminium plate, the stability and performance were consistent with those of the other materials.

References

Anderson, R. J. and Spong, M. W. 1989. Bilateral control of teleoperators with time delay. *IEEE Transactions on Automatic Control* 34:494–501.

Armstrong, B., Khatib, O., and Burdick, J. 1986. The explicit dynamic model and intertial parameters of the puma 560 arm. In *Proc. of the Int. Conf. on Robotics and Automation*, pp. 510–518.

Cortesão, R. 2002. *Kalman Techniques for Intelligent Control Systems: Theory and Robotic Experiments*. PhD thesis, University of Coimbra.

Cortesão, R., Park, J., and Khatib, O. 2003. Real-time adaptive control for haptic manipulation with active observers. In *Proc. of the Int. Conf. on Intelligent Robots and Systems (IROS)*, Las Vegas.

Daniel, R. and McAree, P. 1998. Fundamental limits of performance for force reflecting teleoperation. *International Journal of Robotics Research* 17(8):811–830.

Diolaiti, N., Niemeyer, G., Barbagli, F., Salisbury, K., and Melchiorri, C. 2005. The effect of quantization and coulomb friction on the stability of haptic rendering. In *Proceedings of IEEE World Haptics Conference*.

Erickson, D., Weber, M., and Sharf, I. 2003. Contact stiffness and damping estimaation for robotic systems. *International Journal of Robotics Research* 22(1):41–57.

Franklin, G. F., Powell, J. D., and Emami-Naeini, A. 2002. *Feedback Control of Dynamic Systems, 4th edition*. Prentice Hall.

Freund, E. 1975. The structure of decoupled nonlinear systems. *Int. J. Contr.* 21(3):443–450.

Hannaford, B. 1989. A design framework for teleoperators with kinesthetic feedback. *IEEE Transactions on Robotics and Automation* 5:426–434.

Hashtrudi-Zaad, K. and Salcudean, S. E. 2002. Transparency in time-delayed systems and the effect of local force feedback for transparent teleoperation. *International Journal on Robotics and Automation* 18(1):108–114.

Holmberg, R. and Khatib, O. 2000. Development and control of a holonomic mobile robot for mobile manipulation tasks. *International Journal of Robotics Research* 19(11):1066–1074.

Khatib, O. 1987. A unified approach for motion and force control of robot manipulators: The operational space formulation. *Int. J. on Robotics and Automation* 3(1):43–53.

Khatib, O. and Burdick, J. 1986. Motion and force control of robot manipulators. In *Proceedings of the International Conference on Robotics and Automation*, pp. 1381–1386.

Khatib, O., Sentis, L., Park, J., and Warren, J. 2004. Whole-body dynamic behavior and control of human-like robots. *Int. J. of Humanoid Robotics* 1(1):29–43.

Kim, W. S., Hannaford, B., and Bejczy, A. K. 1992. Force-reflecting and shared compliant control in operating telemanipulators with time delay. *International Journal on Robotics and Automation* 8:176–185.

Lawrence, D. 1993. Stability and transparancy in bilateral teleoperation. *IEEE Trans. on Robotics and Automation* 9(5):624–637.

Love, L. and Book, W. 1995. Environment estimation for enhanced impedance control. In *Proc. of the Int. Conf. on Robotics and Automation*, pp. 1854–1859.

Niemeyer, G. and Slotine, J. 1991. Stable adaptive teleoperation. *IEEE Journal of Oceanic Engineering* 16(1):152–162.

Niemeyer, G. and Slotine, J. 2004. Telemanipulation with time delays. *The International Journal of Robotics Research* 23:873–890.

Ryu, J., Kwon, D., and Hannaford, B. 2004. Stable teleoperation with time-domain passivity control. *IEEE Transactions on Robotics and Automation* 20(2):365–373.

Seraji, H. and Colbaugh, R. 1997. Force tracking in impedance control. *International Journal of Robotics Research* 16(1):97–117.

Singh, S. and Popa, D. 1995. An analysis of some fundamental problems in adaptive control of fooorce and impedance behavior: Theory and experiments. *IEEE Transactions on Robotics and Automation* 11(6):912–921.

Yokokohji, Y. and Yoshikawa, T. 1994. Bilateral control of master-slave manipulators for idela kinesthetic coupling. *IEEE Transactions on Robotics and Automation* 10:605–620.

Zhu, W. and Salcudean, S. 2000. Stability guaranteed teleoperation: An adaptive motion/force control approach. *IEEE Transactions on Automatic Control* 45(11):1951–1969.